(Revision 2) Size distributions of nanoparticles from magnetotactic bacteria as signatures of biologically controlled mineralization

Petr Jandacka[1,2,*], Petr Alexa[2,3], Jaromir Pistora[1], Jinhua Li[4], Hana Vojtkova[5], Ales Hendrych[1,2]

[1]Nanotechnology Centre and IT4Innovations Centre, VŠB-Technical University of Ostrava, Ostrava, Czech Republic

[2]Institute of Physics, VŠB-Technical University of Ostrava, Ostrava, Czech Republic

[3]Institute of Clean Technologies, VŠB-Technical University of Ostrava, Ostrava, Czech Republic

[4]Paleomagnetism and Geochronology Laboratory, Key Laboratory of Earth´s Deep Interior, Institute of Geology and Geophysics, Chinese Academy of Sciences, Beijing 100029, China

[5]Institute of Environmental Engineering, VŠB-Technical University of Ostrava, Ostrava, Czech Republic

Abstract

This paper addresses the problem of magnetite nanoparticle size distributions in magnetotactic bacteria. The methods described in the paper can be used to determine the origin of natural magnetite nanoparticle samples. We analyzed 36 histograms related to bacterial, inorganic and biomimetic nanoparticle sizes. Using statistical software we concluded that the size of the nanoparticles in cultured magnetotactic bacteria follows an extreme value distribution. Magnetite in uncultured samples can be treated as a two-component mixture containing extreme value and/or log-normally distributed nanoparticles. Analysis of the time dependent formation of bacterial magnetite revealed that the magnetite size distribution transforms from

* Address: 17. listopadu 15/2172, 70833 Ostrava, Czech Republic. E-mail: petr.jandacka@vsb.cz

the initial log-normal (young bacterial culture) through normal-like toward the extreme value distribution (evolved culture). It seems that at a certain moment during bacterial magnetite formation, the bacterial system starts to behave as a closed system. The closing of the system must be followed by another unknown process, because restriction of the nutrient supply into magnetosomes is insufficient for the generation of the extreme value distribution. Based on our analysis, approximately 50% of the magnetite particles in the Martian meteorite ALH 84001 follow an extreme value distribution.

Keywords: biomineralization, magnetite, magnetotactic bacteria, meteorite ALH 84001, extreme value

INTRODUCTION

Magnetic nanoparticles (crystals) play an important role in the space orientation of magnetotactic bacteria (Bazylinski and Frankel, 2004). They are produced intracellularly during a complicated biomineralization process controlled by proteins (Faivre and Schuler, 2008; Komeili, 2012), and comprise ferrimagnetic magnetite (Fe_3O_4) or greigite (Fe_3S_4) coated with biomembrane (so-called magnetosomes). The approximate size of the magnetic nanoparticles is 20–120 nm, which is the size range of stable magnetic single-domains. The preference for stable single-domain crystals facilitates the orientation of magnetotactic bacteria in the geomagnetic field. Particles smaller than 20–30 nm are superparamagnetic at ambient temperature and at isolated states (Muxworthy and Williams, 2009), while isolated particles larger than 120 nm naturally create magnetic multi-domains (Muxworthy and Williams, 2006). Magnetite nanocrystals exist in various shapes, from isometric to elongated and combinations of cubes {100}, dodecahedrons {110} and octahedrons {111} (Bazylinski

and Frankel, 2004). Highly elongated bacterial magnetite crystals were observed and described recently (Lefevre et al., 2011; Li et al., 2010).

In the previous two decades, many papers dealing with magnetite from magnetotactic bacteria have focused preferentially on crystal morphology, and secondarily on (almost all only qualitatively) the size distribution of magnetite nanoparticles as potential biomarkers of crystal origins (Arató et al., 2005; Devouard et al., 1998; Han et al., 2007; Meldrum et al., 1993; Pósfai et al., 2001). Accumulated data, presented as histograms of nanoparticle size measurements from transmission electron microscopy (TEM) images, span both cultivated and uncultured bacterial samples. From robust data analyses it was concluded that bacterial magnetite nanoparticle distributions have negative skewness, contrary to the well-known positive skewness of synthetic distributions that follow the log-normal distribution (Eberl et al., 1998; Faivre et al., 2005; Han et al., 2007). Extracellular magnetite nanoparticles created via biologically induced mineralization also follow the log-normal distribution (Frankel and Bazylinski, 2003; Frankel and Buseck, 2000) and can be nucleated by both passive and active mechanisms (Perez-Gonzalez et al., 2010). However, the complex statistical analysis of particle size distributions (including appropriate statistical function fitting) has been virtually ignored despite being a requirement of some studies (Devouard et al., 1998; Faivre et al., 2005; Faivre and Zuddas, 2006). Exceptions are Pósfai et al. (2001), who fitted measured histograms for magnetotactic bacteria containing greigite crystals using the GALOPER code (see Discussion) for inorganic crystal growth and Arató et al. (2005), who tested whether two biogenic samples come from the same distribution using the χ^2 test.

In this paper, a comprehensive statistical analysis of bacterial magnetite nanoparticle sizes is presented for the first time. We aim to determine whether biogenic magnetite nanoparticle sizes follow a typical statistical distribution function that can serve as a

characteristic marker of their biogenic origin in natural sediments and subsequently to understand better the crystallization pathway of bacterial magnetite.

METHODS OF DATA ANALYSIS

Using Corel Draw X3 software, we processed histograms presented in several reports of bacterial magnetite nanoparticle size measurements graphically. The measurements were (in original works) performed using the ellipse-fit method (Devouard et al., 1998) or direct measurement of one dimension (crystal length or width) using TEM or high resolution TEM (HRTEM). These histograms are related to the cultured magnetotactic bacteria strains *Magnetospirillum magnetotacticum* (M.m. strain MS-1), MV-1, MC-2, MSR-1, MV-2 and MV-4 (recognized as MMS-1) and uncultured samples designated S4S, Séd and S3S (Arató et al., 2005; Devouard et al., 1998; Han et al., 2007; Meldrum et al., 1993). The uncultured bacterial samples came from the natural environment (river, pond or sea water). Additionally, one original dataset of bacterial magnetite crystal sizes for the cultured *Magnetospirillum magneticum* strain AMB-1, related to the time dependent formation of the crystals, was processed directly (for more details see original paper Li et al., 2009). For comparison, several abiotic and biomimetic laboratory prepared magnetite samples were also analyzed from published histograms (Arakaki et al., 2010; Faivre et al., 2005; Han et al., 2007). Finally, two histograms representing Martian magnetite from meteorite ALH 84001 were analyzed (Golden et al., 1997). MatLab 7.0 and Statgraphics Centurion XVI statistical and fitting toolboxes were used to identify the best fitting distributions for the published histograms and data. During the analysis, a set of basic two-parametric statistical distribution functions was applied (see Table 1). In total, we processed probability fits on 36 histograms: 11 bacterial, 8 inorganic (abiotic), 5 biomimetic and 12 obtained from the original magnetite size measurements for AMB-1 at different stages of the culture evolution.

Specifications of methods used

Method A (statistical fit of probability densities): After the graphical processing of histograms using the Corel Draw software, uniform data within every original histogram bin were generated based on measured frequencies in the bin. We then processed the data using Statgraphics and MatLab software. The software automatically transformed the original histograms to a probability density function (PDF). This method was used to calculate basic statistical parameters, to evaluate the statistical significance of the fit by the Kolmogorov-Smirnov test (evaluating the maximal differentiation between the experimental and theoretical cumulative distribution function (CDF) to set the significance level *p*-value, where the number 0 indicates statistical insignificance and 1 maximal significance) and to evaluate the goodness-of-fit (by the log-likelihood parameter: advanced goodness of fit number evaluating the difference between experimental data and a theoretical curve; the higher the number, the better the fit of the experimental data).

Method B (statistical fit of cumulative distributions): Experimental CDFs were derived from the original histograms using the Corel Draw software. Such CDFs are affected by relatively small error (for details see Table 2). The three best fits obtained from Method A were fitted by the CDFs using MatLab 7.0. The goodness of fit was characterized by the reduced χ^2 parameter (for explanation see notes below Table 4). This method is typically more precise than Method A.

Method C: Original datasets for strain AMB-1 were processed directly using the above-mentioned software.

Note: For evaluation of the goodness of fit, the advanced parameters χ^2 (Matlab 7.0) and log-likelihood (Statgraphics Centurion XVI) were used. Within the simplest auxiliary analyses, the R^2 number was computed (enumerating the relative minimal difference of a

square deviations sum between experimental data and theoretical fit, where $R^2 = 1$ indicates the best fit).

Uncertainties estimation

The standard uncertainty of the relative frequencies of the individual bins can be estimated using equation $u_{hi} = (u_A^2 + u_B^2 + u_C^2 + u_D^2)^{0.5}$ (for more details see Table 2). In the evaluation of the goodness of fit, only the graphical uncertainty u_D was taken into account while the other uncertainties (u_A, u_B and u_C) were neglected.

RESULTS

Size distributions of magnetite crystals in magnetotactic bacteria

Basic statistical parameters

In Fig. 1, a basic graphical statistical summary is presented using box-plots. The interquartile range of the samples spans an interval from 8 nm (the smallest interquartile range for MV-1 bacterial strains) to 38 nm (the largest interquartile range for the uncultured Séd sample). All interquartile ranges are within the single magnetic domain size range. Only a small number of particles in a few samples reach sizes extending into the superparamagnetic or multi-domain zone.

In Table 3, the characteristics and basic statistical parameters of the investigated bacteria distributions are summarized. The most interesting parameter is the skewness. All bacterial samples exhibit negative skewness, while synthetic Fe_3O_4 has positive skewness. The sign of skewness is the first robust parameter that can be used to distinguish between samples of biogenic and non-biogenic origin (Arató et al., 2005; Faivre et al., 2005).

Fitting of the experimental distributions

The three best fits, as determined by Method A, are presented in Fig. 2a (an example for MS-1). The fit of the CDFs assessed from Method B is displayed in Fig. 2b. In Table 4, the goodness of fit and its statistical significance as obtained from Methods A and B are summarized. Because Method B provides a more exact fit (no approximation is used) we computed location and scale parameters of the best-fit distribution function and their extended uncertainties (95% confidence level) with this method.

It appears that the experimental histograms of cultured bacterial magnetite are best described by the two-parametric extreme value distribution with high statistical significance level, whereas for the uncultured samples (see Figs. 3 and 4), S4S and Séd, this distribution is statistically insignificant. The curve shape of the uncultured S3S sample follows the normal-like distribution. The synthetic Fe_3O_4 particle size follows the log-normal distribution closely, as has been confirmed in other studies (Eberl et al., 1998; Faivre et al., 2005; Han et al., 2007).

Size distributions of magnetite crystals growing in abiotic and biomimetic environments

Using Method B in combination with the computation of R^2, which characterizes the goodness of fit, we analyzed other histograms presented in papers related to the biomimetic (Arakaki et al., 2010) or abiotic (Faivre et al., 2005; Han et al., 2007) crystallization of magnetite crystals.

Abiotic magnetite nanoparticles were prepared by Han et al. (2007) and Faivre et al. (2005), who studied magnetite crystallization in different total iron concentrations (TIC, TIC regimes 0.009, 0.018, 0.06, 0.12 and 0.18 M). According to our statistical analysis, all these abiotic magnetites follow the log-normal distribution as expected. Only in the case of the most concentrated sample (TIC 0.18 M) in Faivre et al. (2005) is the crystal size distribution more

symmetric and the nanoparticles follow a normal distribution slightly better than the log-normal one.

The biomimetic magnetite syntheses (solution 1 ml: 30 mM $FeSO_4 \cdot 7H_2O$, 100 mM KOH, and 400 mM KNO_3) studied by Arakaki et al. (2010) show various magnetite distributions depending on proteins or peptides (50 μg/ml) influencing magnetite crystallization. According to our analysis, in the case of the crystallization in the presence of protein Mms6 or GLM6B, nanoparticles follow the Weibull distribution; in the presence of GLM6A or M6A, the logistic one; and in the presence of M6B, the log-normal one. The experimental nanoparticles crystallized in the absence of a bio-factor follow the symmetric Laplace distribution.

Decomposition of histograms of the uncultured samples

As mentioned above, the experimental magnetite nanoparticle size of the uncultured S4S, Séd and S3S are fitted poorly by the extreme value distribution. We propose that the nanoparticle size distributions can be decomposed into two CDFs using a new five-parametric function:

$$\mathrm{CDF} = a \cdot \mathrm{CDF}_1(x, \mu_1, \sigma_1) + (1 - a) \cdot \mathrm{CDF}_2(x, \mu_2, \sigma_2), \quad (1)$$

where the real parameter $a = \langle 0, 1 \rangle$ is related to the number of particles in the first distribution, CDF_1 and CDF_2 are log-normal (Logn) or extreme value (Ev), μ and σ are location (mean) and scale (variance) parameters (for details see notes under Table 1). We now assume that the S4S, Séd and S3S samples are mixtures containing particles from different growth processes: (i) two strains (CDF_1 is Ev and CDF_2 is Ev), (ii) bacterial log-normally distributed magnetite is present in addition to the bacterial extreme value component (CDF_1 is

Logn and CDF_2 is Ev) or (iii) only bacterial log-normal magnetite is present (CDF_1 is Logn and CDF_2 is Logn).

To test the validity of our approach, we fitted the artificially mixed data sample Mix from Arató et al., (2005) containing biogenic (negative skewed distribution) and synthetic (log-normally distributed) nanoparticles of known parameters (see Figure 10b and Table 1 in the paper Arató et al., 2005). Note: the authors incorrectly denoted the sample as a mix of their samples SYN1+S1 but it is actually a mix of SYN2+S1A as confirmed by the authors in personal correspondence.

Results of our analysis are summarized in Tables 5 and 6 and in Figs 3 and 4. All estimated parameters in Table 6 coincide with those measured by Arató et al. (2005) within the uncertainty limits that support the validity of our approach.

It should be mentioned that our analysis indicates that even magnetite in cultured samples can be treated as a two-component mixture containing extreme value and log-normally distributed nanoparticles. The calculated percentage of the log-normally distributed nanoparticles ranges from 0% (for MV-1) to 31% (for MV-4).

Time-dependence of the bacterial magnetite formation

We evaluated time dependent magnetite formation in the cultured sample of the magnetotactic bacteria *Magnetospirillum magneticum* AMB-1. According to the initial qualitative evaluation, magnetite in AMB-1 passes from a positive skewed (log-normal like) distribution through a symmetric to negative skewed distribution (see Li et al., 2009). We applied Eq. 1 (combination of log-normal and extreme value distribution) to the experimental CDFs of AMB-1. The result is displayed in Fig. 5. It seems that in the initial stage (approx. 28 h incubation), a significant amount (73%) of nanoparticles closely follow the log-normal distribution, then the system passes through a very chaotic region (approx. 40 h incubation)

and terminates (approx. 60 h incubation) in the region where the bacterial concentration in suspension (measured using the optical method) and the percentage of the log-normally (20%) and the extreme value (80%) distributed nanoparticles is approximately constant. Therefore, a significant amount of bacterial crystals following the log-normal distribution may signify a young bacterial culture and a significant amount of crystals following the extreme value distribution may signify an evolved bacterial culture.

Similar observations of time dependent bacterial magnetite formation were performed by other authors (Faivre et al., 2007; Faivre et al., 2010). In Faivre et al. (2010) the formation of magnetite in *Magnetospirillum Gryphiswaldense* strain MSR-1 was investigated and a positive skewed (log-normal like) distribution at the initial stages of the culture growing (up to 110 min) and a negative skewed distribution for the evolved bacterial culture (at 330 min) were observed. These findings are in agreement with our results.

DISCUSSION

Simulation of crystallization processes

GALOPER and experimental distributions

Eberl et al. (1998, 2002) studied the particle size distribution during inorganic crystallization in open and closed systems using the GALOPER code. This code includes basic equations for the Law of Proportionate Effect (LPE, see below), mass balance and Ostwald ripening (Eberl et al., 1998, Kile et al., 2000, Lifshitz and Slyozov, 1961), in which small crystals are dissolved to give matter to the larger crystals thereby minimizing the total free surface energy of the system. Eberl et al. (1998) and Kile et al. (2000) found that crystal size distributions can possess all types of skewness: positive (log-normal and asymptotic), zero (normal) or transitional (bi-modal) and negative, depending on the crystallization conditions. In

experiments conducted with $CaCO_3$, Kile et al. (2000) found that the shape of the crystal size distribution and intensity of the Ostwald ripening process is connected to the level of initial supersaturation of the solution. We think that the level of supersaturation of the solution could influence the results of the above-mentioned experiments related to abiotic and biomimetic magnetite crystallization that were done by Faivre et al. (2005) and Arakaki et al. (2010).

Role of the Ostwald ripening in magnetotactic bacteria

According to our calculations, the negative skewed extreme value distribution of bacterial crystal sizes is noticeably similar to distributions which follow nanoparticles created in a closed system through Ostwald ripening, for which the extreme value distribution is the best two-parametric fit (Fig. 6a). The Ostwald ripening process typically occurs in closed multi-crystallic systems with constant amount of matter (Eberl et al.,1998; Yao et al.,1993). At first sight, it seems improbable that this process plays any role in magnetotactic bacteria, because bacterial magnetites grow in their own reaction vessels (bio-membranes) that contain only one crystal. However, the shape similarity of those two distributions deserves attention.

Hypothetically the magnetite could ripen before the magnetosome membranes are formed, since high supersaturation of solution can induce Ostwald ripening (Kile et al., 2000). This hypothesis disagrees with the observed magnetosome membranes (vesicles) in bacterial body before magnetite formation (Komeili et al., 2004; Murat et al., 2010) and with the initial positive-skewed magnetite distribution observed in youth bacterial cultures (Li et al., 2009; Faivre et al., 2010).

Alternatively, at the time when bacteria start to be closed for external nutrients, inverse Ostwald ripening, observed in Vayssieres et al. (1998) for inorganic magnetite, may commence if magnetosomes are able to communicate chemically through magnetosome filament. This process tends to reach minimal surface energy and keeps the total volume V of

magnetite and number of magnetite crystals in single bacteria constant. In this process, the larger crystals must be dissolved partially to provide matter to the smaller ones so that every single crystal reaches a stable magnetic single domain dimension.

To test the hypothesis of the constant total volume of magnetite typical for Ostwald ripening process and closed systems we extracted the volume V from the crystal size measurements for *Magnetospirillum magneticum* strain AMB-1 (see Fig. 5). We found that V tends to increase continuously even for the evolved bacterial culture in the stationary phase that characterizes dominant negative skewed extreme value distribution (Fig. 6b). It indicates that the Ostwald ripening may not be relevant to the crystallization process in magnetotactic bacteria (see Table 7).

Simulation of crystallization modes in magnetotactic bacteria

Our analysis of the time-dependence of the bacterial magnetite formation indicates that the log-normal distribution is related to the open bacterial system when nutrients may flow toward the growing magnetite crystals (juvenile bacteria). The extreme value distribution is related to the closed bacterial system (full-grown bacteria) beyond the cut-off point, when nutrients are no longer supplied to the magnetosome. The magnetosomes may close separatelly or on the bacterial level. If they close on the bacterial level the average supply of nutrients per crystal must decrease in spite of the fact that the amount of nutrients outside the bacteria could remain constant.

To simulate potential crystallization modes in single bacteria, we generated artificial data for crystal sizes to test if more complicated crystallization processes accompanied by LPE in a supply-controlled system lead, in the final stage, toward negative skewed distribution. The LPE defines the mathematical generation of the linear crystal dimensions (depending on time or number of the crystallization cycles, n) for the supply-controlled

growth by the equation $x_{n+1} = x_n + \beta k x_n$, where k is the random number in the range from 0 to 1, x_n is some specific linear dimension of a crystal, x_{n+1} is its new value and $\beta \in <0,1>$ is the additional variable depending on the volume of nutrients available in cycle n_i (see manual for GALOPER code and Pósfai et al., 2001).

First we tested if a closing bacterial system (where the amount of nutrients for the magnetosomes decreases exponentially to zero, $\beta = \exp(-qn)$ and q is a constant) tends to produce a negative skewed distribution of crystals. In the second test the system was assumed to be open in the initial stage and the amount of nutrients was unrestricted ($\beta = 1$). Next, the system was closed sharply with an exponentially decreasing supply-controlled growth. Our results show that both tests generate significant log-normal distributions (Fig. 7). This indicates that closing the system is an insufficient condition for the generation of a negatively skewed distribution. For this type of distribution, it is necessary to take into account other phenomena such as the role of bio-factors or/and environmental conditions (e.g., Li and Pan, 2012).

Hypothetic crystallization mode in single magnetotactic bacteria

In light of the presented results, observations and considerations, one hypothesis may be stated regarding magnetite crystallization inside bacteria. Subsequent experiments focused on the time dependent formation of the bacterial magnetite and subsequent distribution analysis, and similar to the work by Li et al. (2009) and Faivre et al. (2010), could confirm the following hypothesis:

Initially, magnetite crystals are nucleated in the magnetosome membrane (vesicle) and then grow according to LPE and the system (magnetosome membrane) is opened. The magnetosome membranes are present in bacteria before magnetite nucleation (Komeili et al., 2004). As observed during experiments and confirmed by our analysis, the particles (in single

bacteria) follow the log-normal distribution. The process is controlled by bio-factors and nutrients (iron ions) flow through magnetosome filament managed by cation diffusion facilitator proteins (Uebe et al., 2011) or other proteins (Komeili et al., 2012). Next, bacteria start the final stage of magnetite formation. The magnetosomes are shifted along the filament together when the first crystal reaches the stable magnetic single domain dimension (in MSR-1, Scheffel et al., 2006, Faivre et al., 2010), or appear to be connected permanently with the cell inner membrane (Komeili et al., 2006) and thus are organized into subchains (in AMB-1, Li et al., 2009). Bio-factors stop the crystal growth in some specific dimension (threshold, which is less than the crystal magnetic multidomain dimension) through the prevention of the nutrient supply to the individual membrane (the magnetosome membrane starts to be an individual closed system) or size limitation of the membrane, or both. This threshold may be represented by μ (mode) of the extreme value distribution. Each particle that would exceed the threshold dimension, μ, follows the extreme value distribution and their effective linear dimensions have a variance parameter, σ.

Magnetite distribution in the Martian meteorite ALH 84001

It is well known that, in the Martian meteorite ALH 84001, magnetite crystals in the size range similar to that of the magnetotactic bacteria were observed. Discoverers designated this finding as evidence for ancient life on Mars (McKay et al., 1996). Many authors then started to analyze these meteoritic crystals. They focused typically on the analysis of crystal shapes and several agree (Thomas-Keprta et al., 2000, 2009) while several disagree (Barber and Scott, 2002; Buseck et al., 2001; Golden et al., 2001, 2004) with the hypothesis that the meteoritic magnetite crystals were created by Martian bacteria. However, the crystal shapes do not seem to be reliable biomarkers and over the past sixteen years, the problem has been discussed without any generally accepted conclusion. In response, as a strong biomarker,

which may reveal the biomineralization process and show a difference between bacterial and inorganic crystals, the criterion of crystal size distributions was proposed (Devouard et al., 1998; Faivre et al., 2005; Faivre and Zuddas, 2006). Such analysis, based on CDF fits on Martian magnetite, has not been done up to now.

By applying Method B to the histograms presented in Golden et al (1997) and in combination with Eq. 1, we found parameters of the two component distributions for magnetite crystals in the Martian meteorite (see Fig. 8 and Table 8). We analyzed the samples ALH84001-B (the rim of the carbonate globule, 115 crystals) and ALH84001-C (the whole carbonate globule, 140 crystals). The sample ALH84001-A was not analyzed because of the low number of crystals measured.

It seems that both samples have similar values of fitted parameters μ and σ and contain significant amounts (approx. 50%) of magnetite following the extreme value distribution together with magnetite following the log-normal distribution. We observed such distributions in the case of uncultured bacterial samples and during the evolution of the cultured sample AMB-1, but in light of this paper it is not possible to draw a reliable conclusion about the origin of the magnetite crystals from ALH 84001.

Acknowledgments

Authors thank Mihály Pósfai for information on the sample “Mix” and for other critical comments. This paper was created as part of the projects “IT4 Innovations Centre of Excellence”, Reg. No. CZ.1.05/1.1.00/02.0070, and “Institute of Clean Technologies for Mining and Utilization of Raw Materials for Energy Use”, Reg. No. CZ.1.05/2.1.00/03.0082, and supported by the Research and Development for Innovations Operational Programme financed by the Structural Funds of the European Union and by the state budget of the Czech Republic. The paper was also supported by the National Natural Science Foundation of China

(NSFC 41004024) and the China Postdoctoral Science Foundation (CPSF 201104144) and finally by the project "Study of Magnetic and Surface Properties of Materials", SGS 2012, No. SP 2012/107, from the Ministry of Education, Youth and Sport of the Czech Republic.

References

Arakaki, A., Masuda, F., Amemiya, Y., Tanaka, T., and Matsunaga, T. (2010). Control of the morphology and size of magnetite particles with peptides mimicking the Mms6 protein from magnetotactic bacteria. Journal of Colloid and Interface Science 343, 65-70.

Arató, B., Szanyi, Z., Flies, C., Schuler, D., Frankel, R. B., Buseck, P. R., and Pósfai, M. (2005). Crystal-size and shape distributions of magnetite from uncultured magnetotactic bacteria as a potential biomarker. American Mineralogist 90, 1233-1240.

Barber, D. J., and Scott, E. R. D. (2002). Origin of supposedly biogenic magnetite in the Martian meteorite Allan Hills 84001. Proc Natl Acad Sci U S A 99, 6556-6561.

Bazylinski, D. A., and Frankel, R. B. (2004). Magnetosome formation in prokaryotes. Nature Reviews Microbiology 2, 217-230.

Buseck, P. R., Dunin-Borkowski, R. E., Devouard, B., Frankel, R. B., McCartney, M. R., Midgley, P. A., Posfai, M., and Weyland, M. (2001). Magnetite morphology and life on Mars. Proc Natl Acad Sci U S A 98, 13490-13495.

Devouard, B., Pósfai, M., Hua, X., Bazylinski, D. A., Frankel, R. B., and Buseck, P. R. (1998). Magnetite from magnetotactic bacteria: Size distributions and twinning. American Mineralogist 83, 1387-1398.

Eberl, D. D., Drits, V. A., and Srodon, J. (1998). Deducing growth mechanisms for minerals from the shapes of crystal size distributions. American Journal of Science 298, 499-533.

Eberl et al. (2000): User's guide to GALOPER - a program for simulating the shapes of crystal size distributions and associated programs. U. S. Geol. Survey Open File Report, OF 00-505, 44 p.(ftp://brrcrftp.cr.usgs.gov /pub/ddeberl /pc_version /GALOPER/)

Eberl, D. D., Kile, D. E., and Drits, V. A. (2002). On geological interpretations of crystal size distributions: Constant vs. proportionate growth. American Mineralogist 87, 1235-1241.

Faivre, D., Bottger, L. H., Matzanke, B. F., and Schuler, D. (2007). Intracellular magnetite biomineralization in bacteria proceeds by a distinct pathway involving membrane-bound ferritin and an iron(II) species. Angewandte Chemie-International Edition 46, 8495-8499.

Faivre, D., Fischer, A., Garcia-Rubio, I., Mastrogiacomo, G., and Gehring, A. U. (2010). Development of Cellular Magnetic Dipoles in Magnetotactic Bacteria. Biophysical Journal 99, 1268-1273.

Faivre, D., Menguy, N., Guyot, F., Lopez, O., and Zuddas, P. (2005). Morphology of nanomagnetite crystals: Implications for formation conditions. American Mineralogist 90, 1793-1800.

Faivre, D., and Schuler, D. (2008). Magnetotactic Bacteria and Magnetosomes. Chemical Reviews 108, 4875-4898.

Faivre, D., and Zuddas, P. (2006). An integrated approach for determining the origin of magnetite nanoparticles. Earth and Planetary Science Letters 243, 53-60.

Frankel, R. B., and Bazylinski, D. A. (2003). Biologically induced mineralization by bacteria. Biomineralization 54, 95-114.

Frankel, R. B., and Buseck, P. R. (2000). Magnetite biomineralization and ancient life on Mars. Current Opinion in Chemical Biology 4, 171-176.

Golden, D. C., Thomas-Keprta, K.L, McKay, D.S., Wentworth, S.J, Vali, H., Ming, D.W (1997). Size distribution of magnetite in carbonate globules of ALH84001 Martina meteorite. *28th Annual Lunar and Planetary Science Conference*, p. 427.

Golden, D. C., Ming, D. W., Morris, R. V., Brearley, A., Lauer, H. V., Treiman, A. H., Zolensky, M. E., Schwandt, C. S., Lofgren, G. E., and McKay, G. A. (2004). Evidence for exclusively inorganic formation of magnetite in Martian meteorite ALH84001. American Mineralogist 89, 681-695.

Golden, D. C., Ming, D. W., Schwandt, C. S., Lauer, H. V., Socki, R. A., Morris, R. V., Lofgren, G. E., and McKay, G. A. (2001). A simple inorganic process for formation of carbonates, magnetite, and sulfides in Martian meteroite ALH84001. American Mineralogist 86, 956-956.

Han, L., Li, S., Yang, Y., Zhao, F., Huang, J., and Chang, J. (2007). Comparison of magnetite nanocrystal formed by biomineralization and chemosynthesis. Journal of Magnetism and Magnetic Materials 313, 236-242.

Kile, D. E., Eberl, D. D., Hoch, A. R., and Reddy, M. M. (2000). An assessment of calcite crystal growth mechanisms based on crystal size distributions. Geochimica Et Cosmochimica Acta 64, 2937-2950.

Komeili, A. (2012). Molecular mechanisms of compartmentalization and biomineralization in magnetotactic bacteria. Fems Microbiology Reviews 36, 232-255.

Komeili, A., Li, Z., Newman, D. K., and Jensen, G. J. (2006). Magnetosomes are cell membrane invaginations organized by the actin-like protein MamK. Science 311, 242-245.

Komeili, A., Vali, H., Beveridge, T. J., and Newman, D. K. (2004). Magnetosome vesicles are present before magnetite formation, and MamA is required for their activation. Proc Natl Acad Sci U S A 101, 3839-3844.

Kotz, S., and Nadarajah, S. (2002). "Extreme value distributions: theory and applications.," Imperial College Press, London.

Lefevre, C. T., Posfai, M., Abreu, F., Lins, U., Frankel, R. B., and Bazylinski, D. A. (2011). Morphological features of elongated-anisotropic magnetosome crystals in magnetotactic bacteria of the Nitrospirae phylum and the Deltaproteobacteria class. Earth and Planetary Science Letters 312, 194-200.

Li, J. H., Pan, Y. X., Chen, G. J., Liu, Q. S., Tian, L. X., and Lin, W. (2009). Magnetite magnetosome and fragmental chain formation of Magnetospirillum magneticum AMB-1: transmission electron microscopy and magnetic observations. Geophysical Journal International 177, 33-42.

Li, J. H., Pan, Y. X., Liu, Q. S., Kui, Y. Z., Menguy, N., Che, R. C., Qin, H. F., Lin, W., Wu, W. F., Petersen, N., and Yang, X. A. (2010). Biomineralization, crystallography and magnetic properties of bullet-shaped magnetite magnetosomes in giant rod magnetotactic bacteria. Earth and Planetary Science Letters 293, 368-376.

Li, J., and Pan, Y. (2012). Environmental factors affect magnetite magnetosome synthesis in *Magnetospirillum magneticum* AMB-1: implications for biologically controlled mineralization. Geomicrobiology Journal 29, 362-373.

Lifshitz, I. M., and Slyozov, V. V. (1961). The Kinetics of Precipitation from Supersaturated Solid Solutions. Journal of Physics and Chemistry of Solids 19, 35-50.

McKay, D. S., Gibson, E. K., ThomasKeprta, K. L., Vali, H., Romanek, C. S., Clemett, S. J., Chillier, X. D. F., Maechling, C. R., and Zare, R. N. (1996). Search for past life on Mars: Possible relic biogenic activity in Martian meteorite ALH84001. Science 273, 924-930.

Meldrum, F. C., Mann, S., Heywood, B. R., Frankel, R. B., and Bazylinski, D. A. (1993). Electron-Microscopy Study of Magnetosomes in 2 Cultured Vibrioid Magnetotactic Bacteria. Proceedings of the Royal Society of London Series B-Biological Sciences 251, 237-242.

Murat, D., Quinlan, A., Vali, H., and Komeili A. (2010). Comprehensive genetic dissection of the magnetosome gene island reveals the step-wise assembly of a prokaryotic organelle. PNAS 107(12), 5593-5598.

Muxworthy, A. R., and Williams, W. (2009). Critical superparamagnetic/single-domain grain sizes in interacting magnetite particles: implications for magnetosome crystals. Journal of the Royal Society Interface 6(41), 1207-1212.

Muxworthy, A. R., and Williams, W. (2006). Critical single-domain/multidomain grain sizes in noninteracting and interacting elongated magnetite particles: Implications for magnetosomes. Journal of Geophysical Research 111, 1-7.

Perez-Gonzalez, T., Jimenez-Lopez, C., Neal, A. L., Rull-Perez, F., Rodriguez-Navarro, A., Fernandez-Vivas, A., and Ianez-Pareja, E. (2010). Magnetite biomineralization induced by Shewanella oneidensis. Geochimica Et Cosmochimica Acta 74, 967-979.

Pósfai, M., Cziner, K., Marton, E., Marton, P., Buseck, P. R., Frankel, R. B., and Bazylinski, D. A. (2001). Crystal-size distributions and possible biogenic origin of Fe sulfides. European Journal of Mineralogy 13, 691-703.

Scheffel, A., Gruska, M., Faivre, D., Linaroudis, A., Plitzko, J. M., and Schuler, D. (2006). An acidic protein aligns magnetosomes along a filamentous structure in magnetotactic bacteria. Nature 440, 110-114.

Thomas-Keprta, K. L., Bazylinski, D. A., Kirschvink, J. L., Clemett, S. J., McKay, D. S., Wentworth, S. J., Vali, H., Gibson, E. K., and Romanek, C. S. (2000). Elongated prismatic magnetite crystals in ALH84001 carbonate globules: Potential Martian magnetofossils. Geochimica Et Cosmochimica Acta 64, 4049-4081.

Thomas-Keprta, K. L., Clemett, S. J., McKay, D. S., Gibson, E. K., and Wentworth, S. J. (2009). Origins of magnetite nanocrystals in Martian meteorite ALH84001. Geochimica Et Cosmochimica Acta 73, 6631-6677.

Uebe, R., Junge, K., Henn, V., Poxleitner, G., Katzmann, E., Plitzko, J. M., Zarivach, R., Kasama, T., Wanner, G., Posfai, M., Bottger, L., Matzanke, B., and Schuler, D. (2011). The cation diffusion facilitator proteins MamB and MamM of Magnetospirillum gryphiswaldense have distinct and complex functions, and are involved in magnetite biomineralization and magnetosome membrane assembly. Molecular Microbiology 82, 818-835.

Vayssieres, L., Chaneac, C., Tronc, E., and Jolivet, J. P. (1998). Size tailoring of magnetite particles formed by aqueous precipitation: An example of thermodynamic stability of nanometric oxide particles. Journal of Colloid and Interface Science 205, 205-212.

Yao, J. H., Elder, K. R., Guo, H., and Grant, M. (1993). Theory and simulation of Ostwald ripening. Physical Review B 47(21), 14110-14125.

Table 1. Distributions applied for theoretical analysis (Matlab 7.0 and Statgraphics Centurion XVI).

Name	PDF equation[c]	Skewness	Using (example)
extreme value [a]	$\exp[(x-a)/b]\exp\{-\exp[(x-a)/b]\}/b$	negative	floods frequency
Weibull	$ba^{-b}x^{b-1}\exp[-(x/a)^b]$	all types	lifetime of materials
logistic	$b^{-1}\exp[(x-a)/b]/\{1+\exp[(x-a)/b]\}^2$	zero	feedforward neural networks desc.
normal	$\exp[-(x-a)^2/(2b^2)]/[b(2\pi)^{0.5}]$	zero	frequency of errors
log-logistic	if ln$x$ has a logistic distribution	positive	cancer mortality after diag.
gamma	$x^{a-1}\exp(-x/b)/[b^a\Gamma(a)]$	positive	as Weibull or log-normal
log-normal [b]	$\exp[-(\ln x-a)^2/(2b^2)]/[xb(2\pi)^{0.5}]$	positive	size of particular materials
uniform	$1/(b-a)$	zero	generating of random numbers
Birnbaum-Saunders	if $((x/a)^{0.5}+(a/x)^{0.5})/b$ has a stand. norm. dist.	positive	fatigue life testing of models
inverse Gaussian	$[b/(2\pi x^3)]^{0.5}\exp[-b/(2a^2x)(x-a)^2]$	positive	Brownian motion description
Nakagami	$2(a/b)^a x^{(2a-1)}\exp(-ax^2/b)/\Gamma(a)$	positive	description of an electr. signals
Rician	$I_0(xa/b^2)(x/b^2)\exp[-(x^2+a^2)/(2b^2)]$	positive	communication theory
Laplace	$\exp[-\text{abs}(x-a)/b)]/(2b)$	zero	Brownian motion description

Symbols: $\Gamma(a)$ is the gamma function, a, b are constants, abs(z) denotes absolute value of z and I_0 is the Bessel function of the first kind.

a) $\text{PDF}_{\text{Ev}} = \exp[(x-\mu)/\sigma]\exp\{-\exp[(x-\mu)/\sigma]\}/\sigma$, where μ is the mode and σ is the variance parameter. For other details see ref. Kotz and Nadarajah (2002).

b) $\text{PDF}_{\text{Logn}} = \exp[-(\ln x-\mu)^2/(2\sigma^2)]/[x\sigma(2\pi)^{0.5}]$, where μ is the arithmetic mean and σ is the standard deviation of $\ln(x_i)$ values.

c) PDF = d(CDF)/dx

Table 2. Uncertainty estimation for relative frequencies, h_i, of the individual bins.

	Name	Source	Significance for h_i	max u_{hi} (%) estim.
u_A	TEM or HRTEM resolution[a]	physical limits of individual devices	low	less than 1
u_B	geometry uncertainty	2D crystal shape approximation by ellipse	low	less than 1
u_C	statistical uncertainty	count of crystals measured	low – high	$\sim 1/n_i^{0.5}$ [b]
u_D	graphical uncertainty	width of the histogram lines (in Corel Draw software)	low	2

a) Typical resolution of these modern devices reaches a lattice level (0.1 nm).

b) Number n_i of crystals measured in the individual bin.

Table 3. Basic statistical parameters.

Sample	Sample origin	Shape factor[d] (width/length) and meas. method	Number of crystals per sample	Inter-quartile range	Median	Skewness	Reference
			(-)	(nm)	(nm)	(-)	
M.m.[a]	cultured	0.85-e.f.	229	12	37	− 0.84	(Devouard et al., 1998)
MV-1	cultured	0.65-e.f.	178	8	54	− 1.68	(Devouard et al., 1998)
MC-2	cultured	0.85-e.f.	53	28	91	− 0.92	(Devouard et al., 1998)
Fe_3O_4[b]	synthetic	0.85-e.f.	433	33	42	1.34	(Devouard et al., 1998)
MSR-1	cultured	?-e.f.	100	13	40	− 0.72	(Han et al., 2007)
MV-2	cultured	length	200	16	45	− 0.62	(Meldrum et al., 1993)
MV-4[c]	cultured	length	200	17	62	− 0.56	(Meldrum et al., 1993)
S4S	uncultured	0.6-e.f.	386	16	84	− 1.28	(Arato et al., 2005)
Séd	uncultured	0.9-e.f.	443	38	94	− 0.89	(Arato et al., 2005)
S3S	uncultured	0.7-e.f.	244	15	67	− 0.32	(Arato et al., 2005)

(a) *Magnetospirillum magnetotacticum* (M.m. strain MS-1).

(b) Inorganic.

(c) Recognized as a MMS-1.

(d) Mode of crystals shape factor.

Note: e.f. denotes ellipse fit method of crystal size measurement.

Table 4. Fitting and statistical significance results.

Name	METHOD A		METHOD B			
	Best fit[a] (Log-lik.)$^{p\text{-value}}$	Second-best fit[a] (Log-lik.)$^{p\text{-value}}$	Best fit[b] (red. χ^2)	Second-best[b] fit (red. χ^2)	Location parameter[c] μ (nm)	Scale parameter[c] σ (nm)
M.m. (MS-1)	extreme value $(-826)^{\mathbf{0.99}}$	Weibull $(-840)^{0.13}$	extreme value (22.9)	Weibull (108)	39.90 ± 0.49	7.70 ± 0.58
MV-1	extreme value $(-582)^{\mathbf{0.97}}$	Weibull $(-589)^{0.69}$	extreme value (7.70)	Weibull (18.5)	55.46 ± 0.32	4.91 ± 0.38
MC-2	extreme value $(-231)^{\mathbf{0.99}}$	Weibull $(-234)^{0.77}$	extreme value (135)	Weibull (396)	96.64 ± 0.94	17.14 ± 1.12
Syn. Fe_3O_4	Birnb.-Saund. $(-1981)^{0.52}$	log-normal $(-1982)^{\mathbf{0.73}}$	log-normal (18.3)	-	3.72 ± 0.01	0.56 ± 0.01
MSR-1	extreme value $(-367)^{\mathbf{0.99}}$	Weibull $(-370)^{0.63}$	extreme value (237)	Weibull (1046)	42.26 ± 0.65	8.25 ± 0.77
MV-2	extreme value $(-770)^{\mathbf{0.99}}$	Weibull $(-772)^{0.32}$	extreme value (9.80)	Weibull (69.1)	47.74 ± 0.42	9.47 ± 0.50
MV-4 (MMS-1)	Weibull $(-781)^{0.37}$	extreme value $(-782)^{\mathbf{0.98}}$	extreme value (17.5)	Weibull (33.6)	65.65 ± 0.51	10.29 ± 0.60
S4S	extreme value $(-1539)^{\text{n.s.}}$	Weibull $(-1568)^{\text{n.s.}}$	extreme value (77.7)	Weibull (128)	86.67 ± 1.40	10.90 ± 1.65
Séd	extreme value $(-2032)^{\text{n.s.}}$	Weibull $(-2077)^{\text{n.s.}}$	extreme value (57.1)	Weibull (136)	99.12 ± 1.57	22.05 ± 1.87
S3S	Weibull $(-961)^{0.80}$	logistic $(-962)^{\mathbf{0.99}}$	logistic (5.90)	normal (7.80)	67.40 ± 0.30	7.01 ± 0.27

(a) Log-lik. denotes Log-likelihood. *p*-value (according to Kolmogorov-Smirnov test) less than 0.05 indicates that bacterial nanoparticles do not come from the selected distribution with 95% confidence. The abbreviation n.s. denotes “not significant”.

(b) The reduced χ^2 value equals $\chi^2 = \Sigma_i[(y_i - y_{i\,\mathrm{fit}})^2/(u_i^2)]/(N - f - 1)$, where $u_i = u_D n^{-1}[i(1 - \mathrm{CDF})^2 + (N - i)\mathrm{CDF}^2]^{0.5}$ is the uncertainty of the experimental CDF-value y_i in the i-th bin, u_D (see Table 2) is the measured graphical extraction uncertainty of the particle number in individual bins, n is the total number of particles in the histogram, N is the number of the fitted points (bins) and f is the number of the fitted coefficients.

(c) On the 95% confidence level for the best fit of Method B.

Table 5. Decomposition of uncultured samples by Eq. 1.

Name	2 parametric	5 parametric (mixed fits using Eq. 1)				
	Best fit[a] (red. χ^2)	Best fit[a] (red. χ^2)	Second-best[a] (red. χ^2)	Nanopart. type (%)[b] log-normal	extreme value	Result (bacteria strain estimation)[c]
S4S	Ev (77.7)	Logn + Ev (1.03)	Logn + Logn (15.8)	23	77	one-strain bacterial sample (?)
Séd	Ev (57.1)	Ev + Ev (4.26)	Logn + Ev (8.91)		30+70	two strains of bacteria (? + MC-2)
S3S	logistic (5.90)	Logn + Ev (1.92)	Logn + Logn (3.95)	43	57	one-strain bacterial sample (MV-4?)
Mix[d]	-	Logn + Ev (43.4)	Logn + Logn (299)	83	17	inorganic and bacterial magnetite (S1A)[e]

(a) The reduced χ^2 value calculated as for Table 4.

(b) Nanoparticle composition in the samples determined according to parameter a in Eq. 1.

(c) Bacterial strain estimation according to the fitted parameters from Eq. 1 (? stands for impossible strain determination).

(d) Control sample for determination of the method validity.

(e) See Arató et at. (2005).

Table 6. Comparison of parameters for the sample Mix.

Parameters	Measured	Calculated[a]
synthetic particles (%)	77	83 ± 10
biogenic particles (%)	23	17 ± 10
mode of log-normal[b] (synthetic) (nm)	50	50 ± 3
mode of extreme value (biogenic) (nm)	120	115 ± 5

(a) On the 95% confidence level for the best fit of Eq. 1. Fitted parameters: log-normal (a = 83 ± 10 %, μ_1 = 4.06 ± 0.05, σ_1 = 0.39 ± 0.03) and extreme value (μ_2 = 115.1 ± 5.2 nm, σ_2 = 16.4 ± 8.6 nm).

(b) Mode of the log-normal distribution equals $\exp(\mu_1 - \sigma^2_1)$.

Table 7. Summary of differences between the time dependent Ostwald ripening process and the formation of magnetite crystals in magnetotactic bacteria

	Crystals	Number of crystals	Crystal sizes (nm)	Total volume of crystals	Initial size distribution	Final size distribution	Goal of crystallization
Ostwald ripening	in mutual contact	decreasing	various	constant	various	LSW[a] shape	minimum of interface energy
Bacterial magnetite formation	isolated in bio-membrane	increasing or constant	20-120	increasing	log-normal	extreme value	maximal magnetic moment per bacteria

a) LSW: Lifshitz-Slyozov-Wagner equation for Ostwald ripening (see Eberl et al., 1998):

PDF = $C\cdot(t^{-4/3})\cdot u^2\cdot(3-2u)^{-11/3}\cdot(3+u)^{-7/3}\cdot\exp[3/(2u-3)]$, where C is the scaling constant, t is the time, $u = r/R$, where r is the dimension of crystals and $R = kt^{1/3}$ is the mean dimension of crystals (k is a constant).

Table 8. Parameters for magnetite crystals in Martian meteorite ALH 84001 according to Eq. 1.

	Best fit (red. χ^2)	Second-best fit (red. χ^2)	Third-best fit (red. χ^2)	Fit parameters (%, nm)		Result
				log-normal (a; μ_1; σ_1)	extreme value ({1-a}; μ_2; σ_2)	
ALH84001-B	Logn+Ev	Ev+Ev	Logn+Logn	36 ± 6	**64** ± 6	significant amount (64%)
	(0.81)	(13.6)	(191)	3.35 ± 0.04	**48.23** ± 0.78	of bacterial-like
				0.49 ± 0.04	**11.38** ± 0.94	magnetite
ALH84001-C	Logn+Ev	Ev+Ev	Logn+Logn	54 ± 7	**46** ± 7	significant amount (46%)
	(1.26)	(14.5)	(36.3)	3.48 ± 0.03	**48.76** ± 1.51	of bacterial-like
				0.50 ± 0.03	**12.02** ± 1.59	magnetite

Note: For statistical details see Tables 4 and 5.

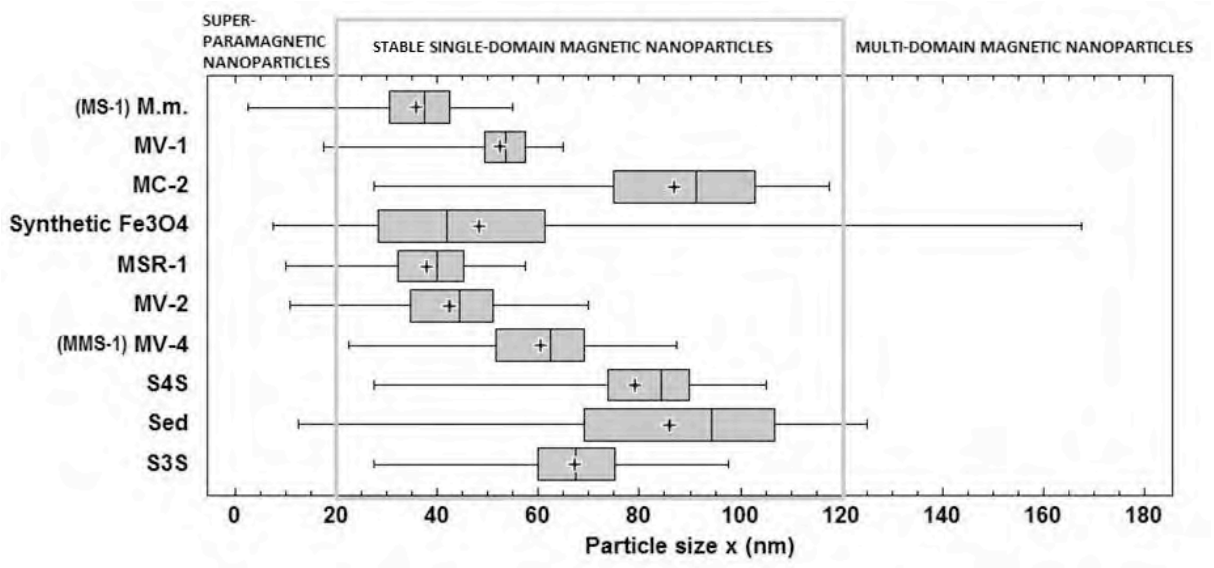

Figure 1**.** Box-plot for bacterial and inorganic magnetic nanoparticles. Horizontal bars show the set range, box width along the *x* axis is determined by the $x_{0.25}$ and $x_{0.75}$ quartiles, the middle line in the box and the cross denote median and mean, respectively.

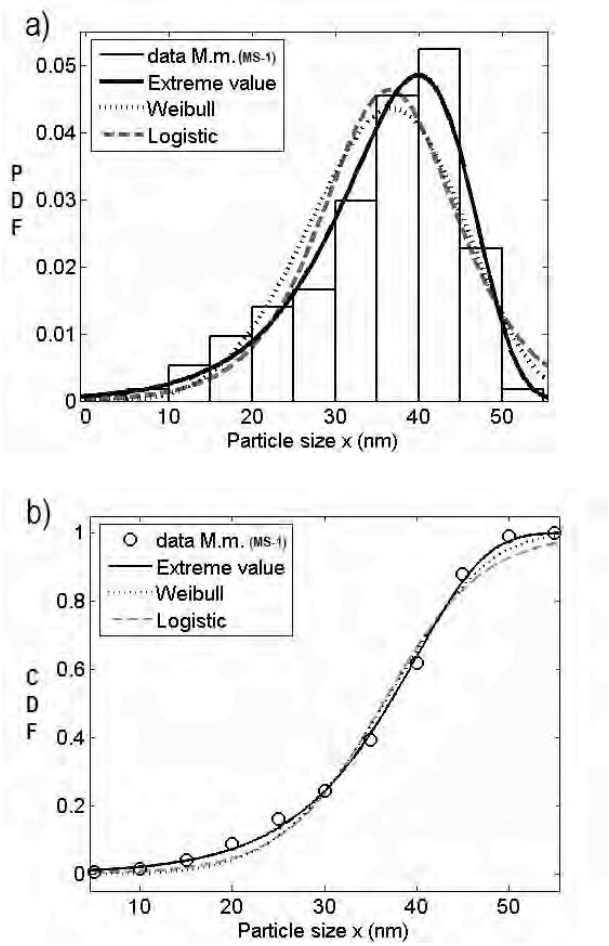

Figure 2. Three best PDF fits of magnetite size distribution in *Magnetospirillum magnetotacticum* (MS-1) determined by Method A (a) and three best CDF fits assessed by Method B (b).

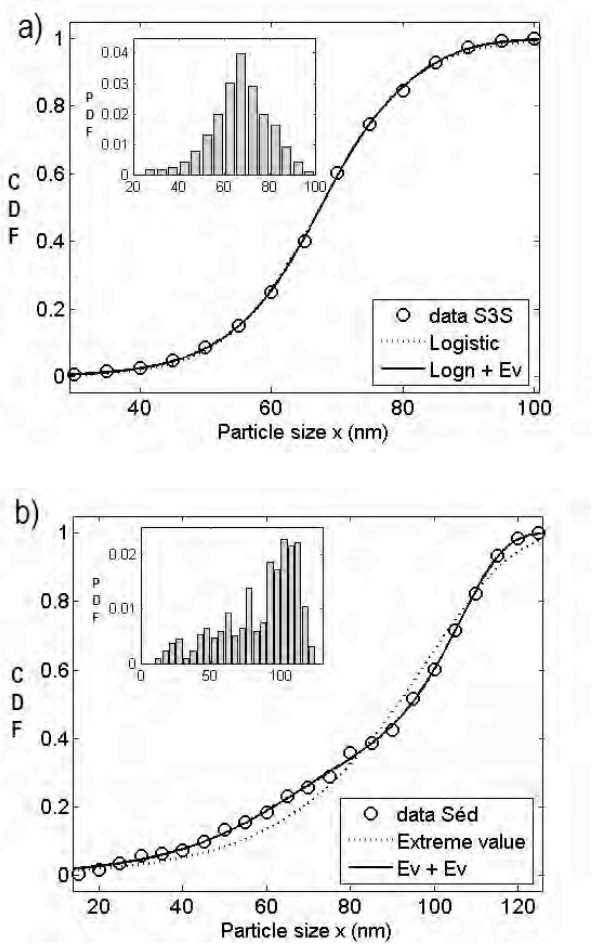

Figure 3. Best two- and five-parametric fits for samples S3S (a) and Séd (b).

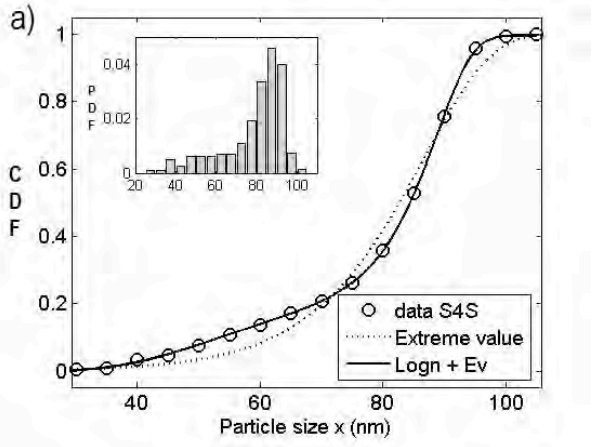

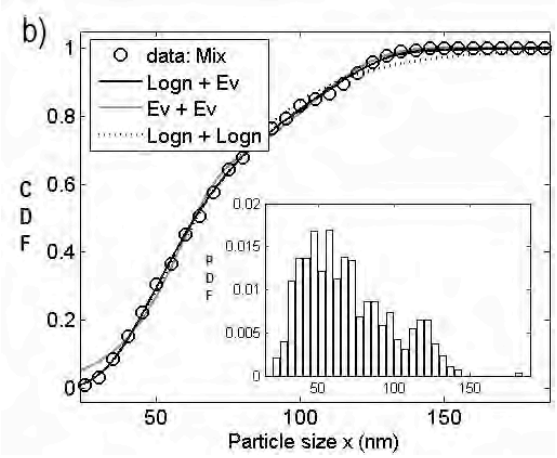

Figure 4. Best two- and five-parametric fits for samples S4S (a) and Mix (b).

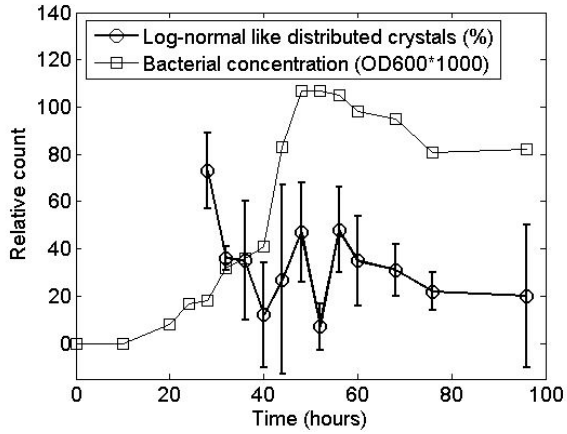

Figure 5. Time dependent representation of hypothetical log-normally distributed magnetite in bacterial sample AMB-1, evaluated according to *a* parameter in Eq. 1 with log-normal and extreme value components (in individual time points at least 193 crystals analyzed). Error bars indicate uncertainties at the 95% confidence level. Bacterial concentration measured according to optical density of suspension by spectrophotometer with 600 nm light (OD600). Data represents the lag, exponential and stationary phases of culture evolution. A significant number of nanoparticles were observed (by TEM) after 28 h.

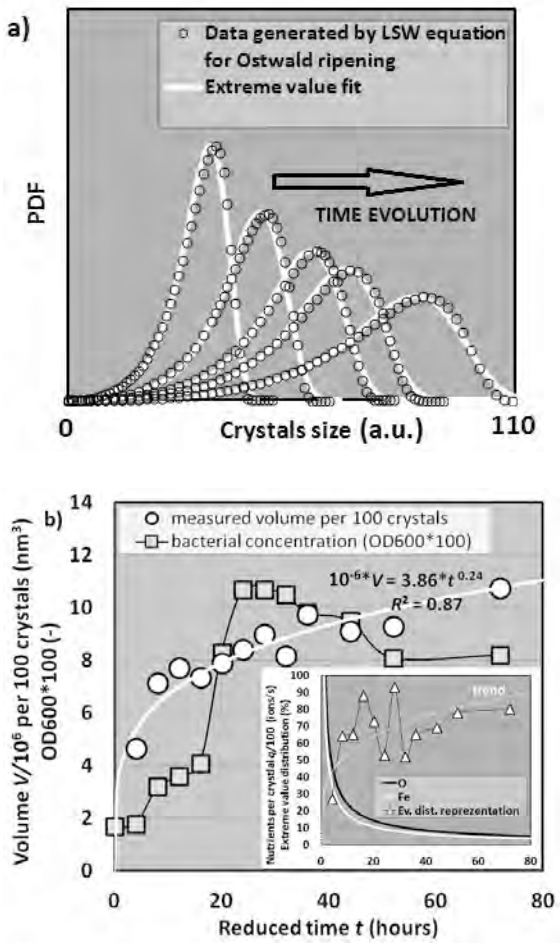

Figure 6. Time evolution of the supply controlled Ostwald ripening according to the LSW equation (see footnotes to Table 7: for $k = 10$ and time points $t_1 = 4$, $t_2 = 10$, $t_3 = 20$, $t_4 = 30$, $t_5 = 60$) fitted by the extreme value distribution (a) and time evolution of 100 crystals from magnetotactic bacteria strain AMB-1 (crystals approximated by cubes, time scale shifted back to the point when the magnetite crystals start to be observed) and of the bacterial concentration (b) (for more details see Fig. 5 caption). Time dependent volume points are fitted by the function $V = 3.86 \cdot 10^6 \cdot t^{0.24}$, where V is the volume per 100 crystals (nm^3) and t is the time (hours). In subplot time evolution of the calculated average flux rates of nutrients (Fe, O) into single crystal and the percentage of the extreme value distributed magnetites are displayed.

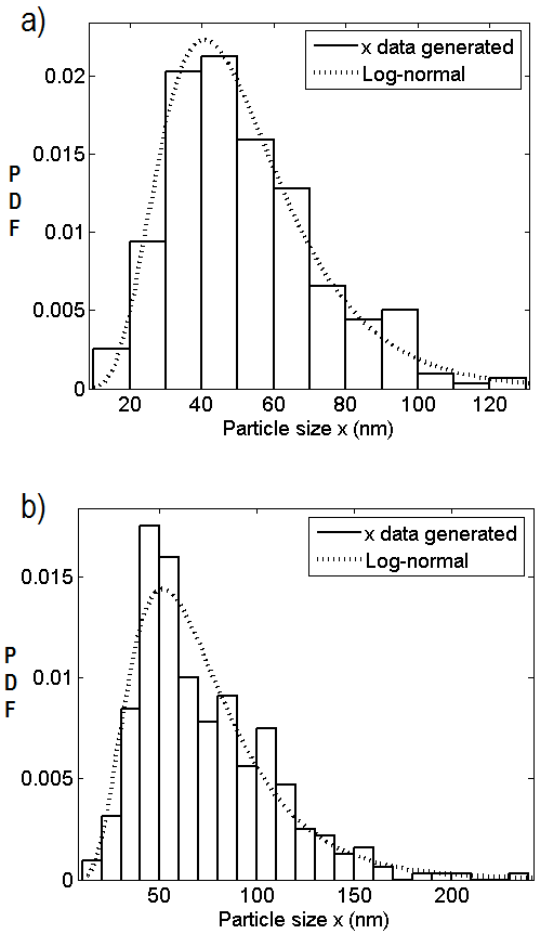

Figure 7. Data generated (320 crystals) using LPE for: single bacteria in the final stage, when amount of nutrients for crystals decreased exponentially to zero (a) and initially opened and subsequently sharply exponentially closing system in the final stage (b). Both crystallization processes lead to the log-normal distribution (*p*-values 0.88 and 0.68).

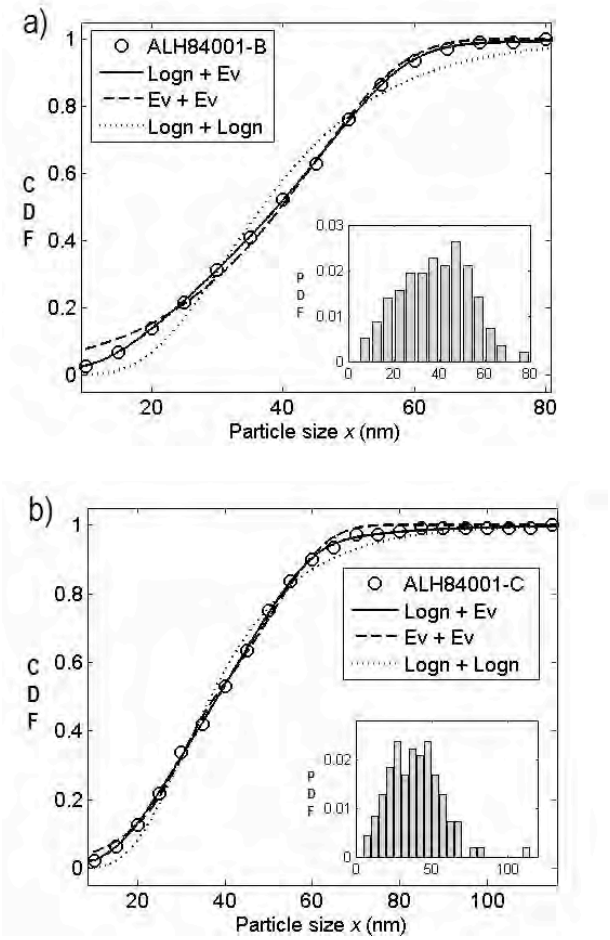

Figure 8. Three fits on measured magnetite CDFs in Martian meteorite, applying Eq. 1: samples ALH 84001-B (a) and ALH 84001-C (b).

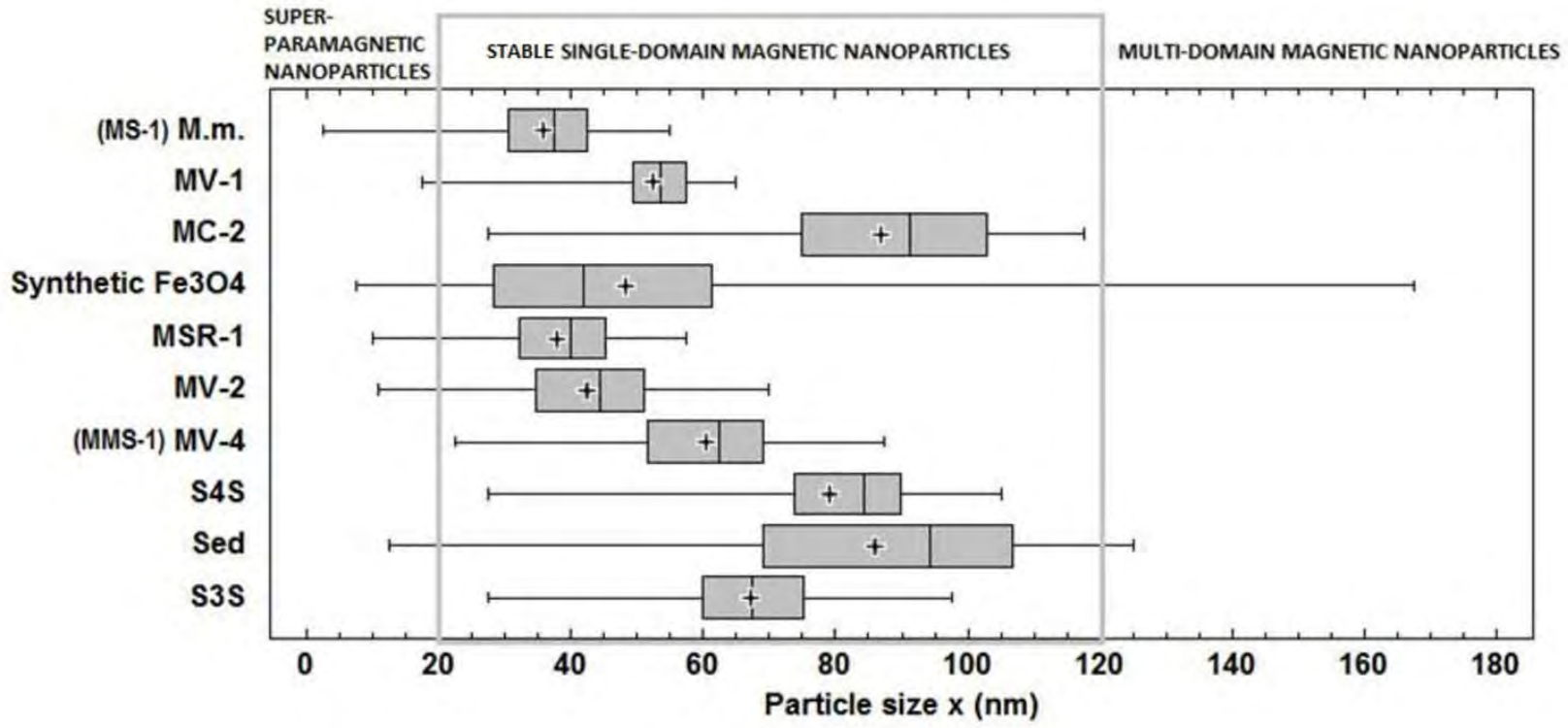
SUPER-
PARAMAGNETIC
NANOPARTICLES
STABLE SINGLE-DOMAIN MAGNETIC NANOPARTICLES
MULTI-DOMAIN MAGNETIC NANOPARTICLES
(MS-1) M.m.
MV-1
MC-2
Synthetic Fe3O4
MSR-1
MV-2
(MMS-1) MV-4
S4S
Sed
S3S
0
20
40
60
80
100
120
140
160
180
Particle size x (nm)

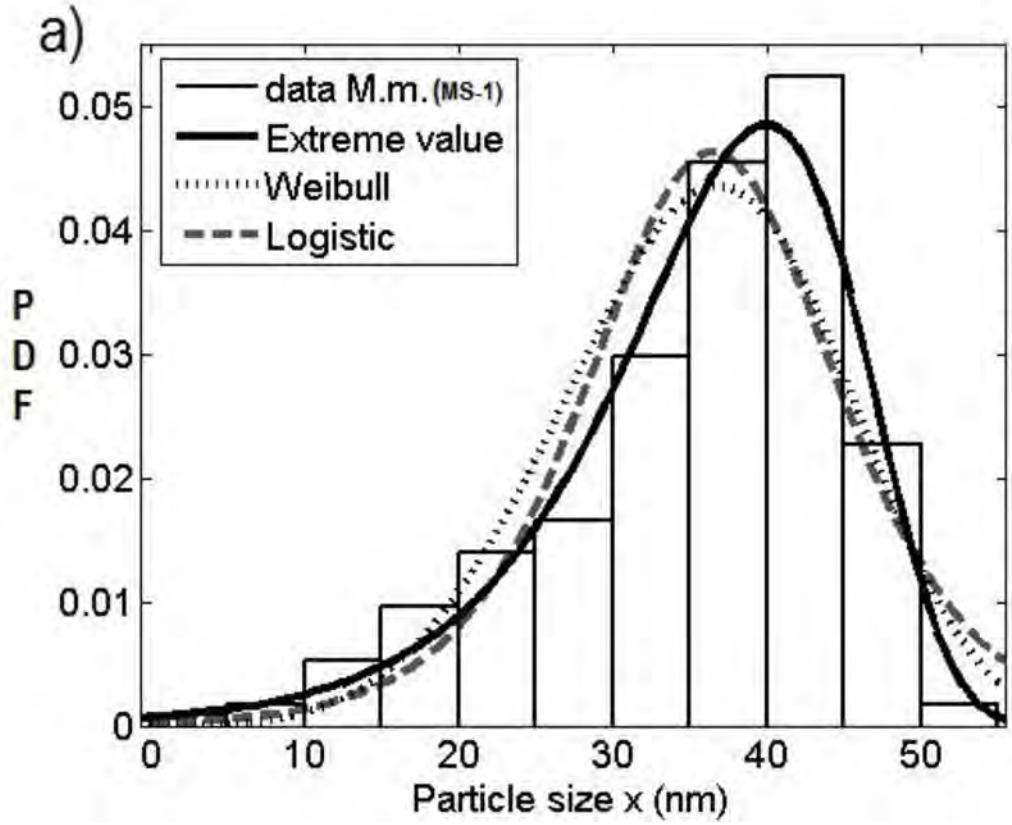
a)
data M.m. (MS-1)
Extreme value
Weibull
Logistic
PDF
0.05
0.04
0.03
0.02
0.01
0
0
10
20
30
40
50
Particle size x (nm)

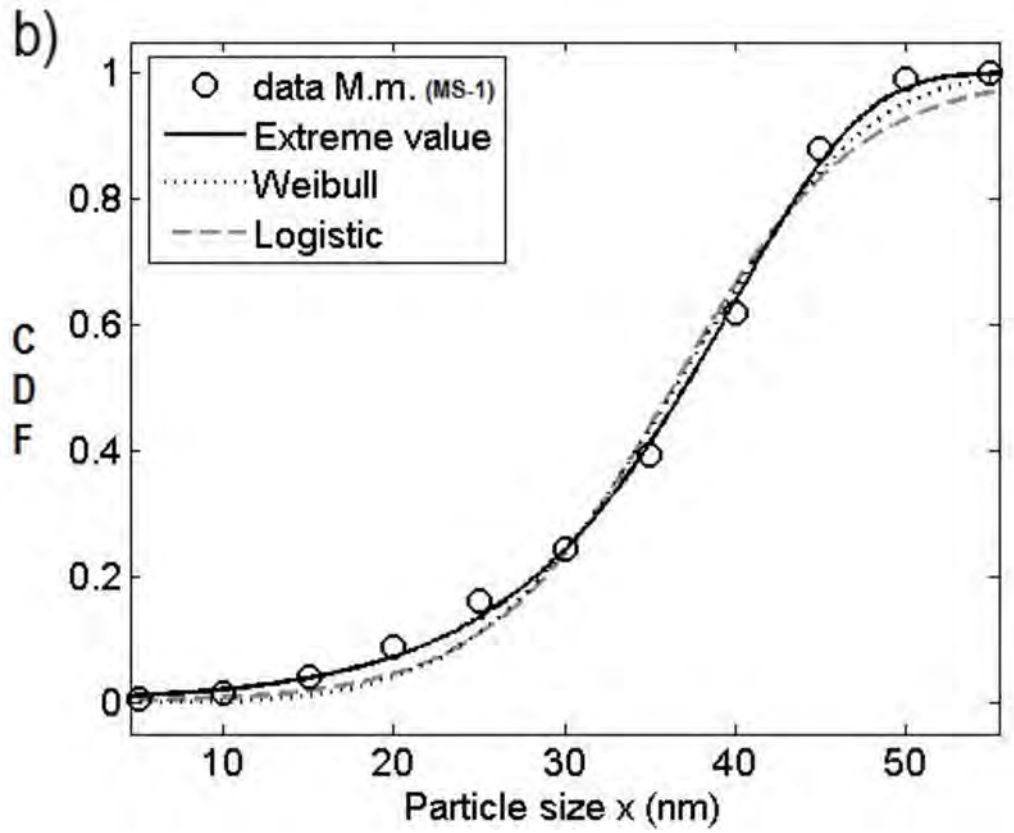
b)
data M.m. (MS-1)
Extreme value
Weibull
Logistic
CDF
0
0.2
0.4
0.6
0.8
1
10
20
30
40
50
Particle size x (nm)

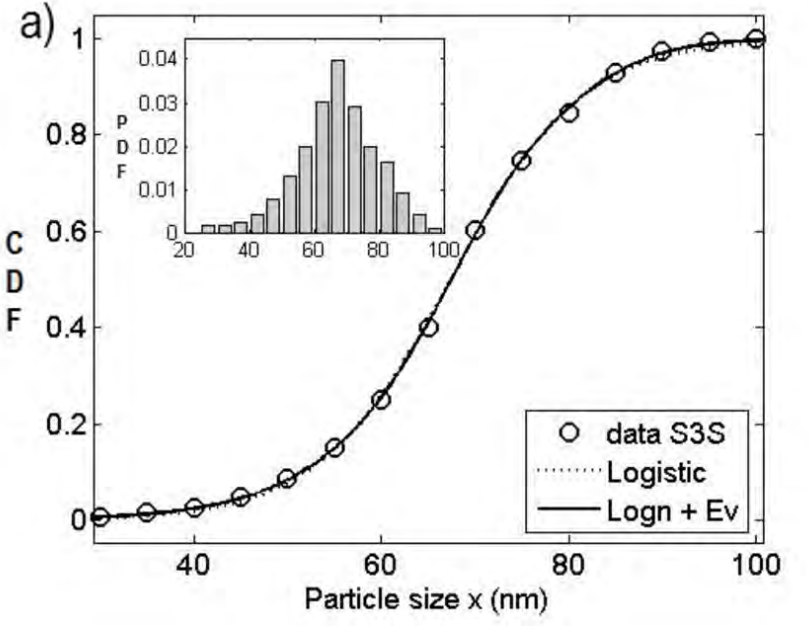
a)
CDF
PDF
Particle size x (nm)
data S3S
Logistic
Logn + Ev
0
0.2
0.4
0.6
0.8
1
20
40
60
80
100
0.01
0.02
0.03
0.04

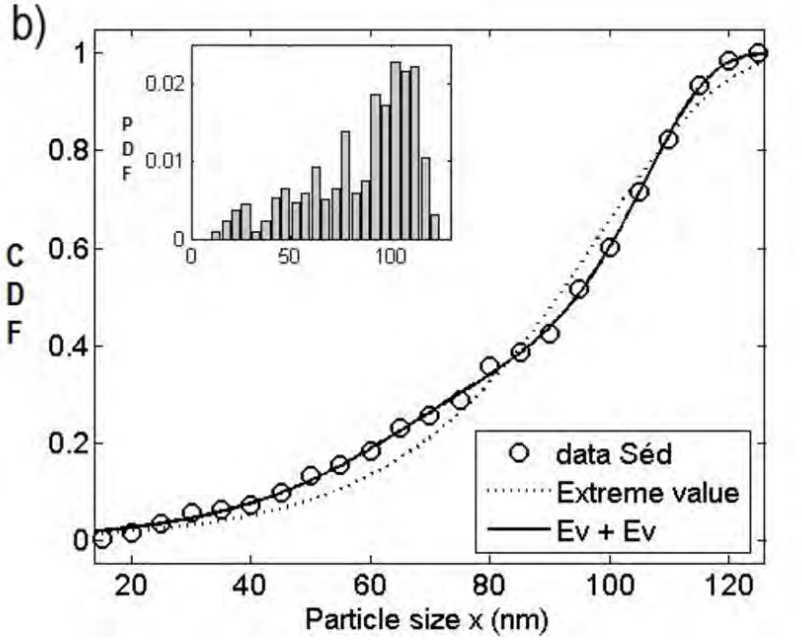
b)
CDF
PDF
Particle size x (nm)
data Séd
Extreme value
Ev + Ev

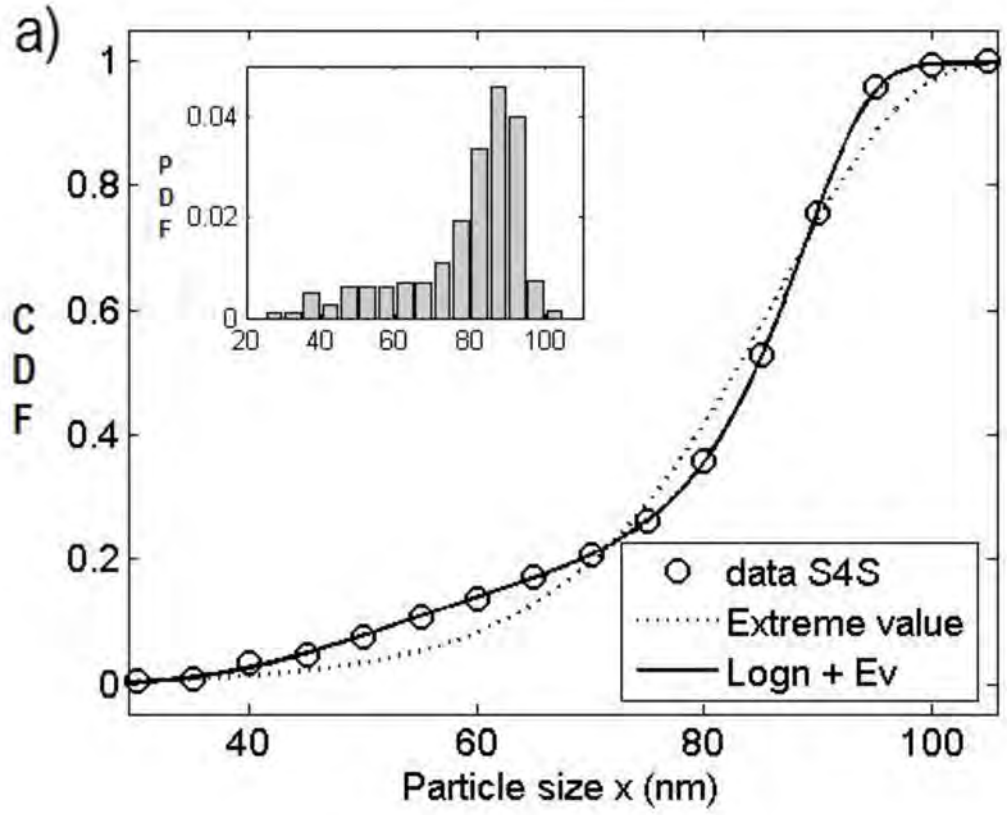
a)
CDF
PDF
Particle size x (nm)
data S4S
Extreme value
Logn + Ev

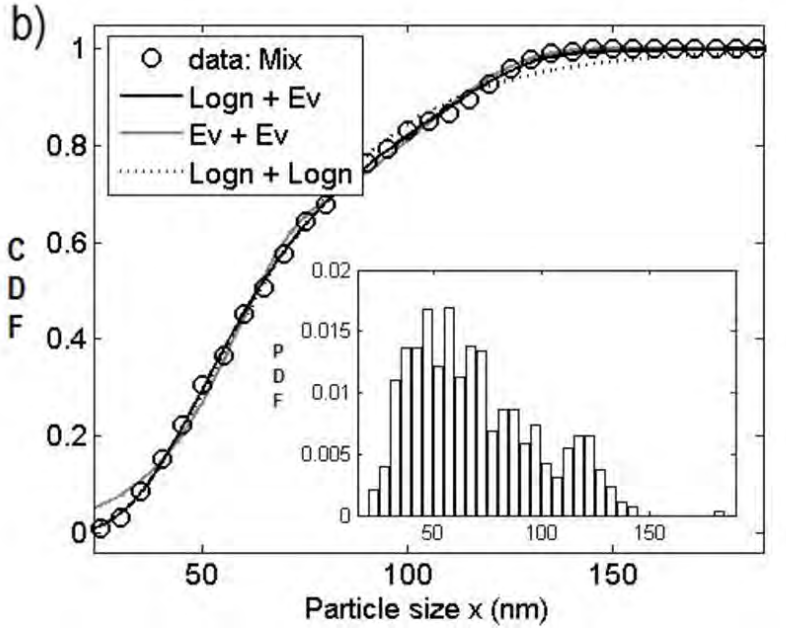
b)
data: Mix
Logn + Ev
Ev + Ev
Logn + Logn
CDF
PDF
Particle size x (nm)
0
0.2
0.4
0.6
0.8
1
50
100
150
0.005
0.01
0.015
0.02

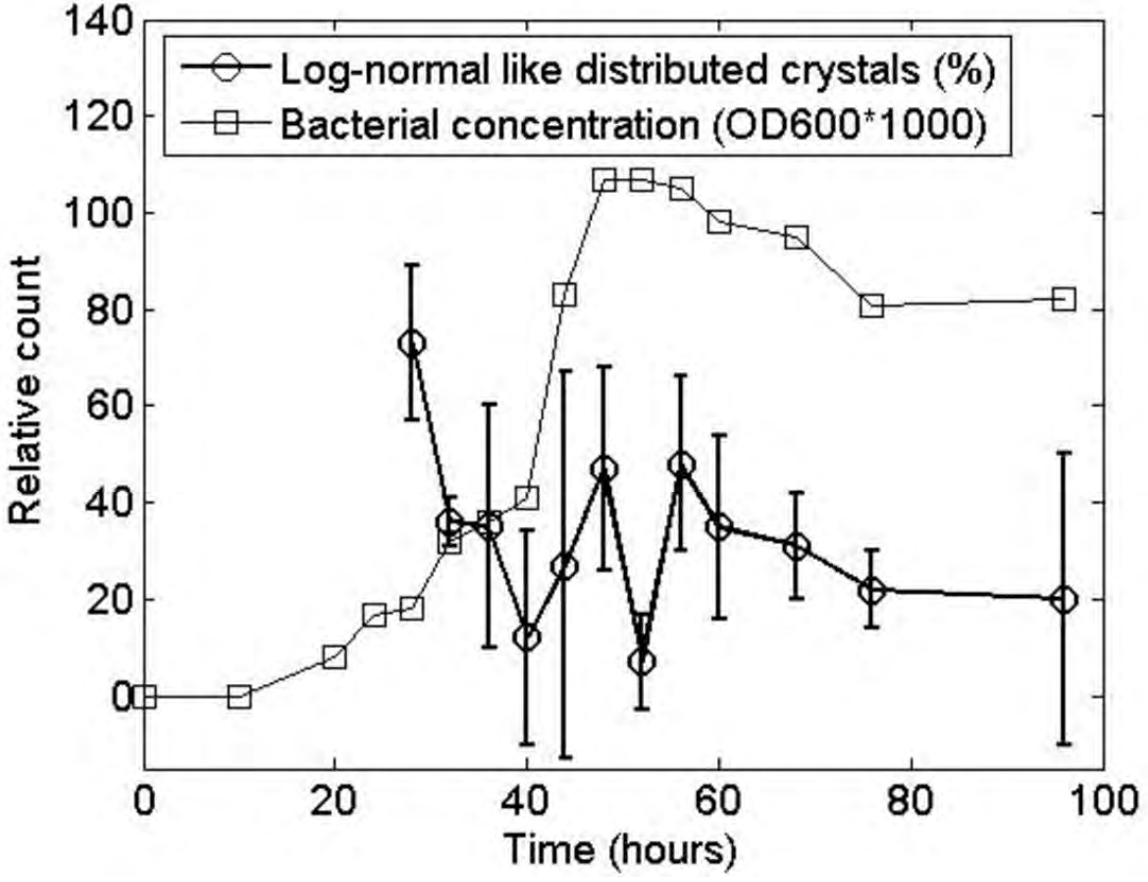
Log-normal like distributed crystals (%)
Bacterial concentration (OD600*1000)
Relative count
Time (hours)
140
120
100
80
60
40
20
0
0
20
40
60
80
100

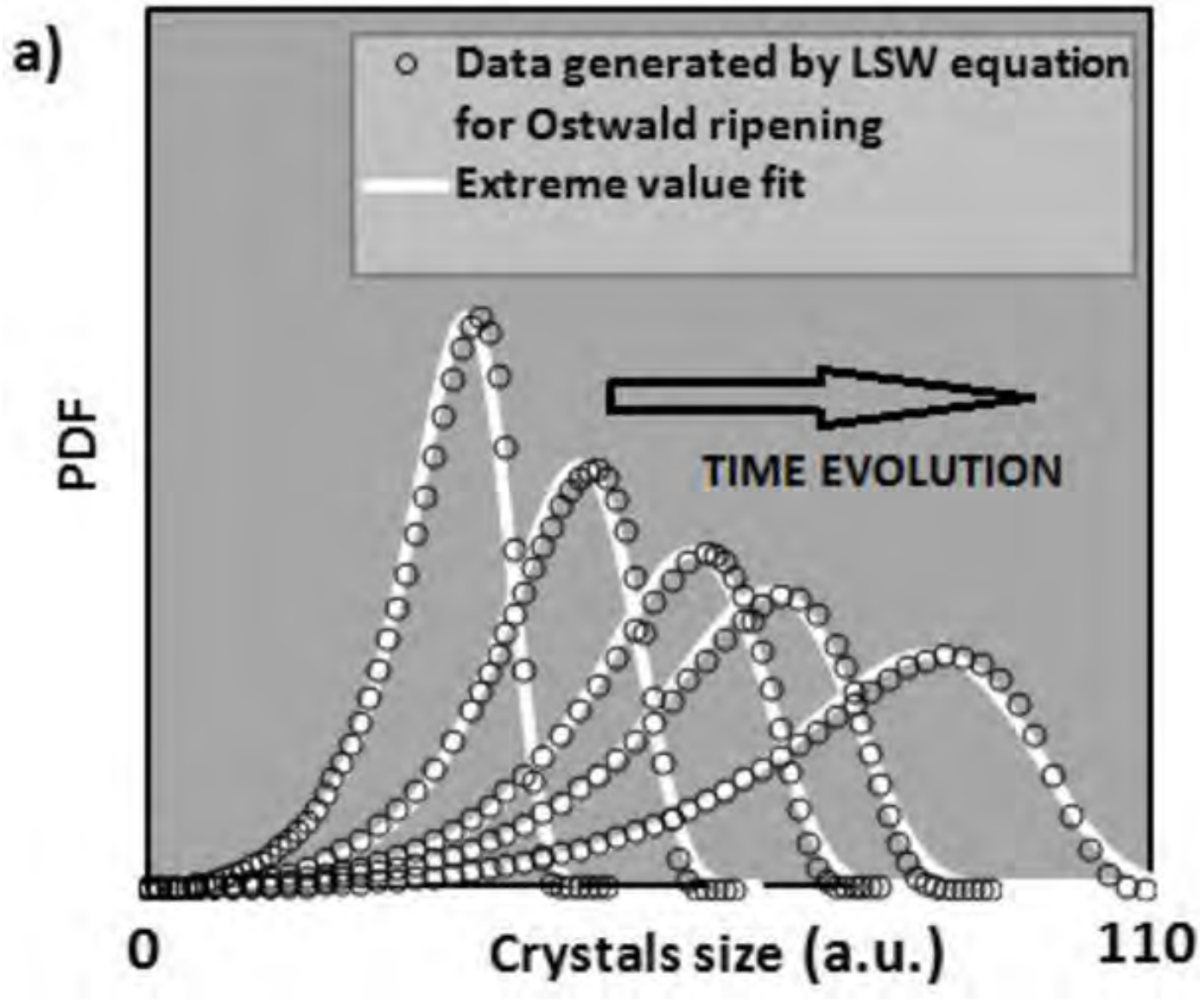
a)
Data generated by LSW equation for Ostwald ripening
Extreme value fit
PDF
TIME EVOLUTION
0
Crystals size (a.u.)
110

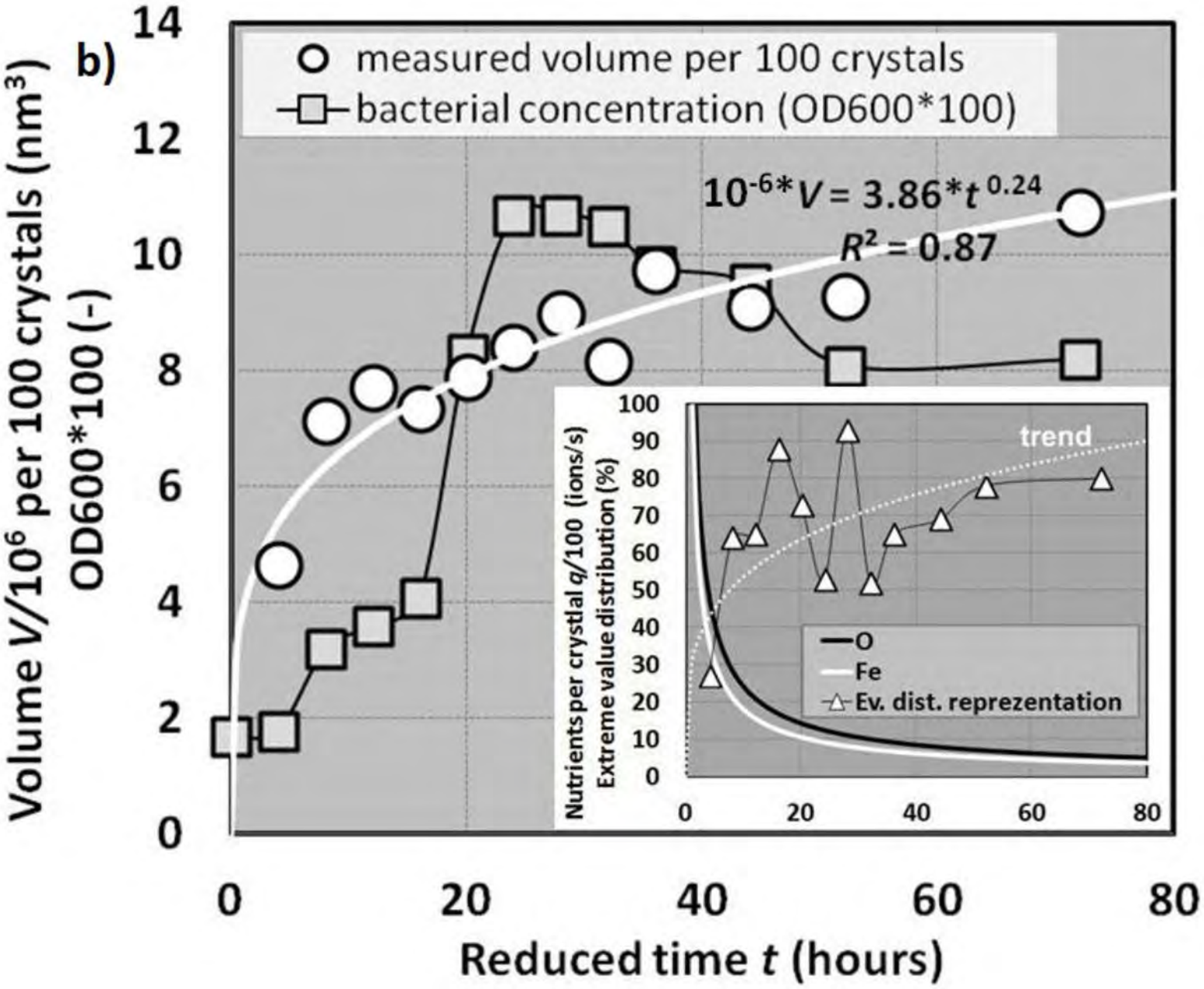
b)
measured volume per 100 crystals
bacterial concentration (OD600*100)
$10^{-6}*V = 3.86*t^{0.24}$
$R^2 = 0.87$
Volume $V/10^6$ per 100 crystals (nm^3)
OD600*100 (-)
Reduced time t (hours)
Nutrients per crystal $q/100$ (ions/s)
Extreme value distribution (%)
trend
O
Fe
Ev. dist. reprezentation
0
2
4
6
8
10
12
14
0
20
40
60
80
0
10
20
30
40
50
60
70
80
90
100

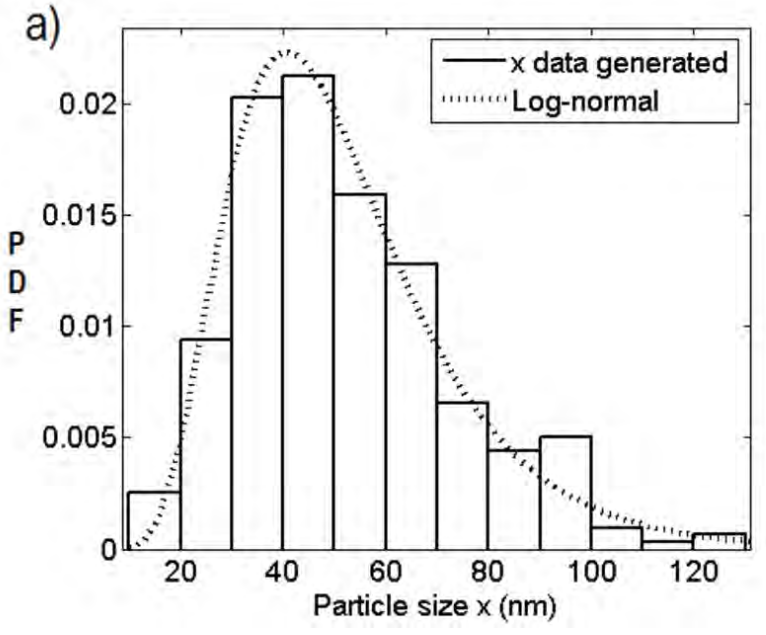
a)
x data generated
Log-normal
0.02
0.015
0.01
0.005
0
P
D
F
20
40
60
80
100
120
Particle size x (nm)

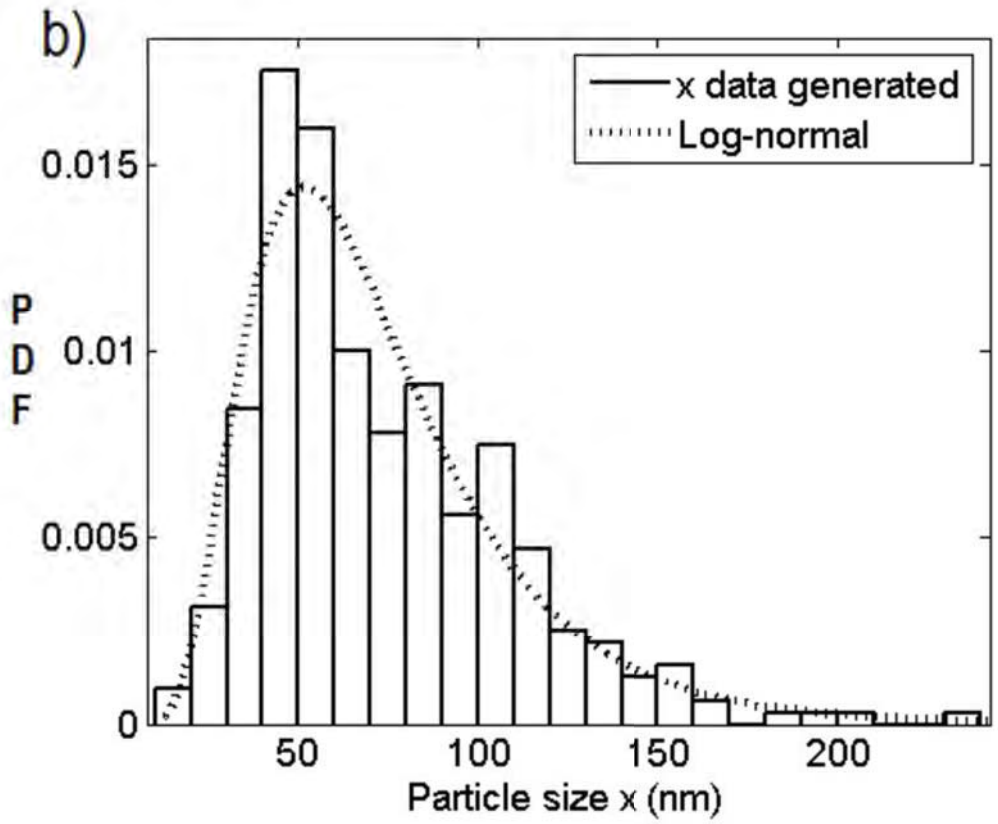
b)
x data generated
Log-normal
0.015
0.01
0.005
0
P
D
F
50
100
150
200
Particle size x (nm)

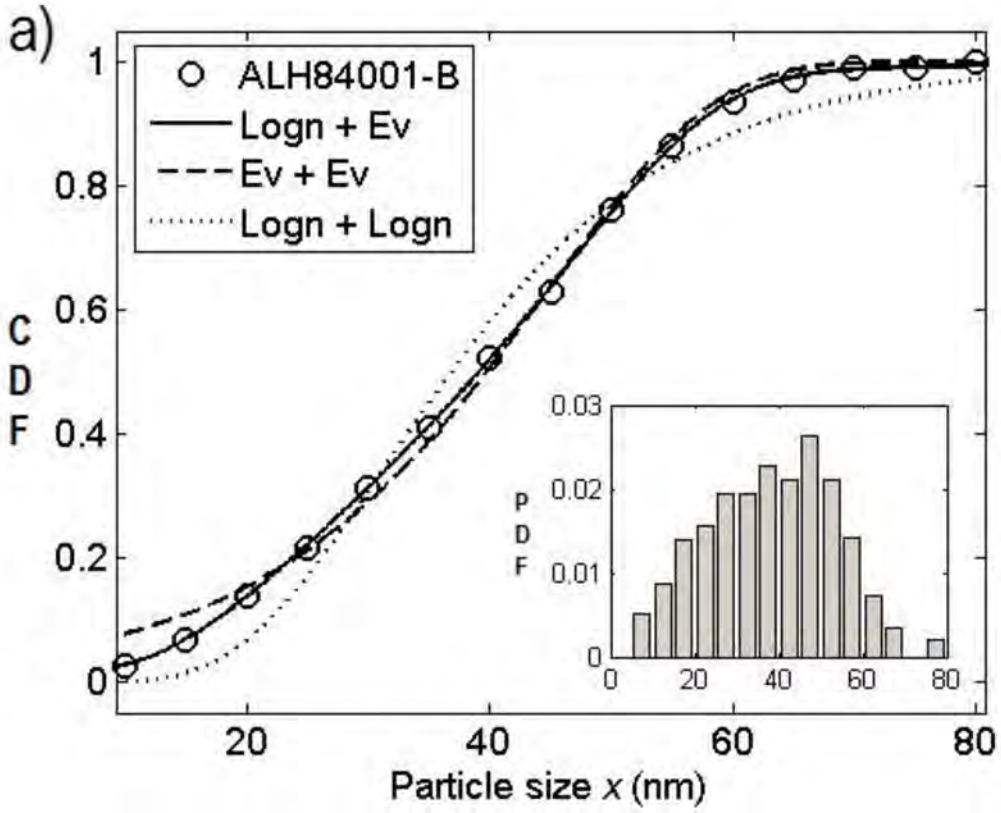
a)
ALH84001-B
Logn + Ev
Ev + Ev
Logn + Logn
CDF
Particle size x (nm)
PDF
0
0.2
0.4
0.6
0.8
1
20
40
60
80
0.01
0.02
0.03

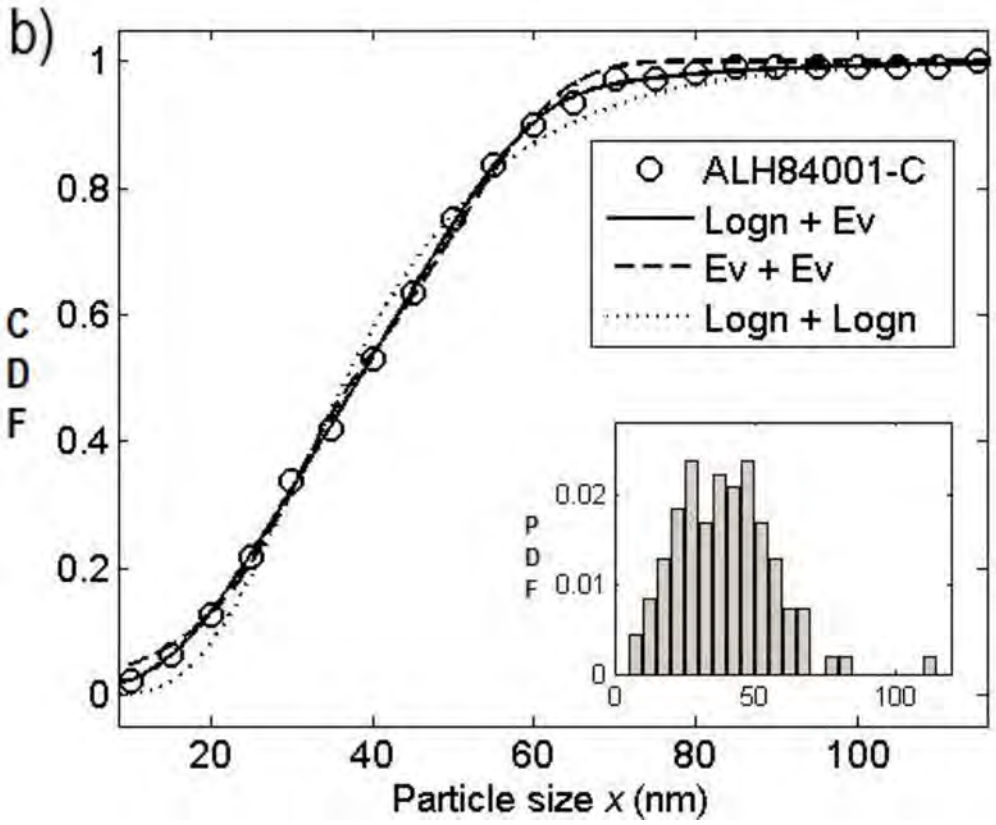
b)
CDF
Particle size x (nm)
ALH84001-C
Logn + Ev
Ev + Ev
Logn + Logn
PDF
0
0.2
0.4
0.6
0.8
1
20
40
60
80
100
0.01
0.02
50